Applied Catalysis B: Environmental 198 (2016) 74–82

Contents lists available at ScienceDirect

Applied Catalysis B: Environmental

journal homepage: www.elsevier.com/locate/apcatb

Catalytic activity of mesoporous cobalt oxides with controlled porosity and crystallite sizes: Evaluation using the reduction of 4-nitrophenol

Batsile M. Mogudi, Phendukani Ncube, Reinout Meijboom *

Department of Chemistry, University of Johannesburg, P.O. Box 524, Auckland Park, Johannesburg 2006, South Africa

ARTICLE INFO

Article history:
Received 29 March 2016
Received in revised form 19 May 2016
Accepted 21 May 2016
Available online 24 May 2016

Keywords:
Heterogeneous catalysts
Mesoporous
Cobalt oxide
4-nitrophenol
Reduction
Crystallite size

ABSTRACT

Mesoporous cobalt oxides were synthesized using an inverse surfactant micelle method. The prepared materials are mono-dispersed nanoparticle aggregates with connected, well defined intra-particle voids. Powder X-ray diffraction, N_2 sorption, scanning electron microscopy and transmission electron microscopy revealed that both pore and nanoparticle sizes are enlarged with thermal treatment temperatures. Nitrogen sorption experiments revealed that the pore diameters increased from 12.1 to 31.9 nm with the final heat treatment increase from 150 to 550 °C. The reduction of 4-nitrophenol has been chosen as a well-controlled model reaction allowing us to determine the catalytic activity as a function of crystallite size and pore diameter. A comparison of the various cobalt oxide catalysts is made in terms of Langmuir-Hinshelwood kinetics.

1. Introduction

The pioneering work on mesoporous materials by Kresge and co-workers [1] as well as by the Stucky research group [2,3] in the 1990s has led to tremendous attention in these materials in a range of applications such as catalysis [4–7], sorption [8–11], gas sensors [12–14] and optics [15–18]. The catalytic activities of mesoporous materials were reported to be superior to their non-porous forms due to their high surface area, nano-crystallinity, mesoporisity, and pore-volume [6]. Mesoporous transition metal oxides such as those of Fe, Co, Mn and Cr were given particular attention due to their multiple oxidation states, resulting in numerous oxides. However, these materials have weak interaction with surfactants, which are conventionally used in the synthesis of mesoporous materials, making the synthesis of mesoporous transition metal oxides difficult [19].

While the synthesis of silica-based mesoporous materials has been well established [20], the synthesis of mesoporous metal oxides remains a challenge. Recently, a report of the successful synthesis of a series of mesoporous materials using an inverse surfactant micelle was used as the soft template to create mesopores instead of using the conventional approach [21]. The sol-gel chemistry was controlled by nitrogen oxide species (NO_x) formed by the thermal decomposition of nitric acid in this synthesis. Treating the resulting gels with different heating cycles resulted in mono-modal, thermally controlled nano-crystalline materials with mesopores between the crystallites. Subsequently, the synthesis of mesoporous cobalt oxide materials using this approach was reported [22], which is difficult to produce using conventional methods.

Here we demonstrate that the mesoporous cobalt oxides prepared by the soft template method [22] can be comprehensively evaluated for their catalytic activity using the reduction of 4-nitrophenol by borohydride in aqueous solution as a model reaction. Nitro-aromatic compounds are toxic organic species which are produced as by-products in the pharmaceutical, agrochemical, urethane, textile and dye chemical industries [23,24]. There is always, therefore, a need to develop economic and green catalysts for the remediation of sources contaminated with these toxic organic compounds by reducing them to the less toxic amines. Precious metals such as palladium and platinum have been used extensively as catalysts [25–28] for this reduction but because these are expensive there is a need to replace these noble metals with non-precious metals such as cobalt.

The reduction of 4-nitrophenol has been intensively used for the evaluation of the catalytic activity of metal nanoparticles in

* Corresponding author.
E-mail address: rmeijboom@uj.ac.za (R. Meijboom).

http://dx.doi.org/10.1016/j.apcatb.2016.05.051
0926-3373/

aqueous suspensions. While most evaluations deal with colloidal metal (Cu, Ag, Au, Pt, Pd, Ru) nanoparticles [29–34], cobalt oxide is also an active catalyst for the reduction of 4-nitrophenol, albeit with low activities [5,24]. Moreover, the mechanism of 4-nitrophenol reduction has been well established and shown to proceed via a Langmuir-Hinshelwood (L-H) model [29,30], that is, both reactants are adsorbed before they react. Thus, the apparent rate constant derived from the kinetic analysis contains not only the rate constant for the reaction of adsorbed species, but also the thermodynamic adsorption constants for both reactants. The reduction of 4-nitrophenol, therefore, presents a well-studied model reaction which is ideally suited for the evaluation of the catalytic activity of new catalysts. We, therefore, give a full kinetic analysis of the heterogeneous-catalyzed reduction of 4-nitrophenol with sodium borohydride using mesoporous cobalt oxide catalysts of varying crystallite size, porosity and surface area. While the heterogeneous catalytic reduction of 4-nitrophenol using cobalt oxide catalysts has been previously reported [5,24], none of these reports give a detailed kinetic analysis of the reaction using mesoporous cobalt oxide catalysts and the catalyst materials previously used were not mesoporous in nature.

2. Experimental

2.1. Materials

All chemicals used were reagent-grade and used as received. Cobalt(II) nitrate hexahydrate [$Co(NO_3)_2{\cdot}6H_2O$], 1-butanol, poly(ethylene glycol)-*block*-poly(propylene glycol)-*block*-poly(ethylene glycol) (PEO20-PPO70-PEO20 or Pluronic P123), sodium borohydride ($NaBH_4$), 4-nitrophenol and morin were purchased from Sigma-Aldrich. Concentrated nitric acid (68–70% HNO_3) was purchased from Rochelle Chemicals (RSA).

2.2. Synthesis of mesoporous cobalt oxides

To synthesize mesoporous cobalt oxides a literature procedure was followed [22]. In short, $Co(NO_3)_2{\cdot}6H_2O$ (10 g, 0.035 mol) was dissolved in a solution containing P123 (5.0 g, 8.62×10^{-4} mol) and HNO_3 (4.8 g, 0.076 mol) in 1-butanol (34 g, 0.66 mol). The red solution was stirred and formed a red gel. The gel was then placed in an oven at 120 °C for 3.5 h. The obtained powder was washed with ethanol several times, and dried in a vacuum oven. The resulting red powders were calcined at 150 °C for 12 h (*meso*-Co-150) and further heated to 250 °C (*meso*-Co-250), 350 °C (*meso*-Co-350), and 450 °C (*meso*-Co-450) and 550 °C (*meso*-Co-550), respectively, for 1 h with a heating rate of 1 °C/min. All heating cycles were performed in air.

2.3. Characterization

Powder X-ray diffraction analyses were performed on a Rigaku Miniflex-600 diffractometer with Cu Kα radiation (λ = 1.5406 Å) at room temperature. Both low angle (2θ = 0.5–8°) and wide angle (2θ = 10–90°) diffraction patterns were measured. Nitrogen sorption measurements were performed on a Micromeritics Tristar 3000 sorption system. The samples were degassed at 90 °C for 18 h prior to the experiments. The surface areas were calculated by the Brunauer-Emmett-Teller (BET) method, and the pore size distributions were obtained by the Barrett-Joyner-Haleda (BJH) method from the desorption branch of the isotherms. Scanning Electron Microscopy (SEM) images were taken on a Tescan Vega 3LMH scanning electron microscope with the samples carbon-coated on copper grids using an Agar Turbo Carbon Coater. High resolution transmission electron microscopy (HRTEM) was performed on a JEOL JEM-2100F electron microscope with an accelerating voltage of 200 kV. Temperature programmed analyses were conducted on a Micromeritics Autochem II. About 30 mg of material was packed in a quartz tube reactor. The loaded samples were pretreated in an inert gas flow (Ar) at 200 °C for 1 h to clean the catalyst surface before each test. Temperature-programmed measurements were performed from room temperature to 800 °C with a heating ramp rate of 10 °C min^{-1}. In H_2-TPR measurements, 10% H_2/Ar was passed through the catalyst bed at a flow rate of 50 ml min^{-1} while the temperature was ramped from 30 °C to 500 °C.

2.4. Catalytic activity

The kinetic evaluation was performed by detecting the extinction of 4-nitrophenol (4NP) *via* UV–vis spectrophotometry using a Shimadzu UV1800 equipped with a CPS-240A Cell Positioner and CPS-Controller for temperature regulation. Stock solutions of 4NP (1000 μM) and $NaBH_4$ (1.0 M) were first prepared. Initial spectrophotometric scans were performed using the full spectrum range of λ 200–800 nm with readings taken every three minutes, in quartz cuvettes. Subsequently all kinetic measurements were performed in disposable polystyrene cuvettes. In a typical run, the appropriate amount of 4NP and catalysts was mixed in a 50 mL jacketed flask and the volume made to 25 mL with deionized water. The mixture was then degassed by bubbling with nitrogen for 30 min. The jacketed flask was then connected to a pre-heated water bath at the desired temperature. Then a 100 fold excess of $NaBH_4$ was added to start the reaction and aliquots of 3 mL were taken at 3 min intervals, filtered and the UV–vis spectrum taken. For the kinetic runs to obtain L-H parameters, two sets of experiments were performed at 25 °C with a constant catalyst amount. The first data set was obtained for a constant $NaBH_4$ concentration while varying the concentration of 4NP. The second set, k_{app} values were obtained for a run were the concentration of $NaBH_4$ was varied while keeping 4-NP concentration constant. For thermodynamic analysis, the temperature of the water bath was varied from 20 to 35 °C. From the raw experimental data, k_{app} values were determined using the Kinetic Studio software [35] while the L-H fitting of the data was performed using the Origin Pro 8.5 graphing and modeling software [36].

3. Results and discussion

3.1. Synthesis and characterization of meso-Co-X catalysts

In this study, we synthesized mesoporous cobalt oxides of varying mesoporisity using a method which involves the use of inverse surfactant micelles as structure-directing agents. The principle behind this method is that sol-gel reactions of the metal oxo-clusters are controlled in acidic medium by NO_x chemistry. Here, NO_x refers to a wide range of nitric oxides formed by the thermal decomposition of the nitrate anion. The formed NO_x species are absorbed on the surface oxo-clusters to prevent uncontrolled condensation and their decomposition increases the pH of the solution, resulting in oxidation of the oxo-clusters. In essence, the *meso*-structured metal oxides are the result of mono-dispersed nanoparticle aggregation and the mesopores are formed by connected intra-particle voids [21]. Characterization of our prepared mesoporous cobalt oxides demonstrated these features.

Powder X-ray diffraction (p-XRD) patterns obtained from low angle and wide angle analysis are shown in Fig. 1(a) and (b), respectively, for the different mesoporous cobalt oxide materials calcined to different final temperatures. All the materials showed a typical spinel Co_3O_4 pattern (JCPDS 090418) with a cubic crystal system. Increasing heat treatment resulted in patterns with sharper diffraction lines, indicating that the particle sizes were increasing with temperature. As shown in the low angle diffraction patterns

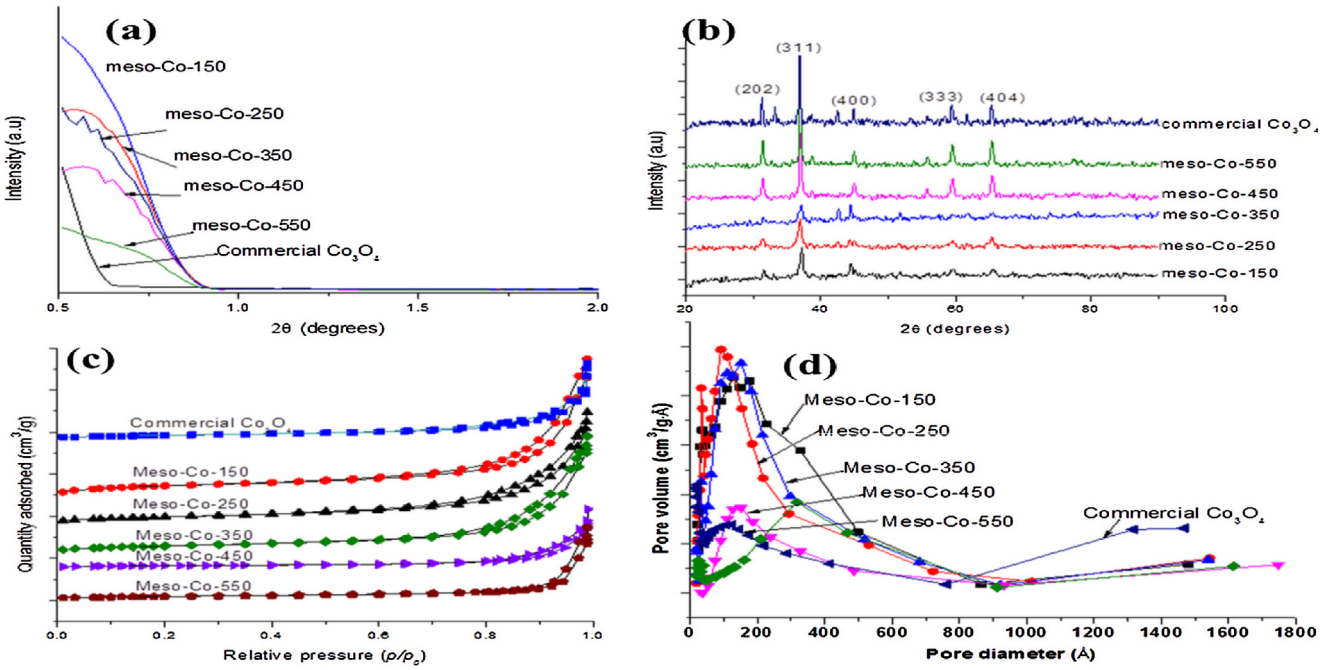

Fig. 1. Characterization of prepared materials: (a) low angle and (b) wide angle p-XRD patterns of *meso*-Co-X (X = 150;250;350;450 and 550 °C) (c) N_2 sorption isotherms and (d) BJH pore size distributions of *meso*-Co-X.

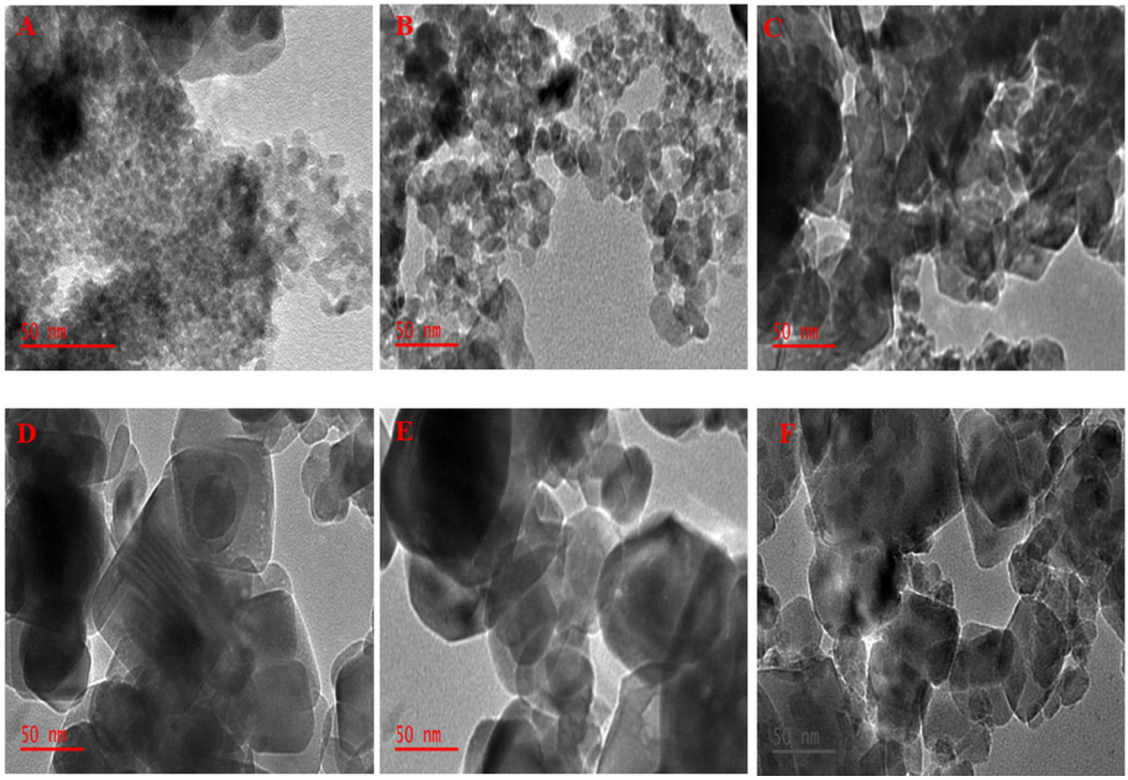

Fig. 2. TEM images of A: *meso*-Co-150, B: *meso*-Co-250, C: *meso*-Co-350, D: *meso*-Co-450, E: *meso*-Co-550 and F: commercial Co_3O_4.

(Fig. 1a) the heat treated samples diffracted in the low angle region, indicating the existence of a *meso*-structured material. The increase in crystallite sizes upon heat treatment can also be observed from TEM analysis (Fig. 2) and SEM analysis (Fig. S1, Supplementary information). The formation of pure Co_3O_4 was also confirmed by EDX analysis which showed peaks for Co and O, with the peak for Cu coming from the copper grids used in the analysis (Fig. S2, Supplementary information).

Nitrogen sorption experiments revealed that the pore diameters increased from 12.1 to 31.9 nm with the final heat treatment increase from 150 to 550 °C as shown in Table 1. All the prepared materials exhibited the characteristic Type IV adsorption isotherms, with a Type I hysteresis loop typical of a regular ordered

Table 1
BET surface areas, BJH pore sizes and pore volumes as well as crystallite sizes[a] of the prepared mesoporous cobalt oxide catalysts and the commercial sample.

Catalyst	BET surface area (m^2/g)	BJH pore size (nm)	Pore volume (cm^3)	Crystallite size[a] (nm)
Meso-Co-150	32.9	12.1	0.093	14.9
Meso-Co-250	29.2	18.3	0.119	16.2
Meso-Co-350	14.2	18.8	0.0870	18.5
Meso-Co-450	12.4	29.9	0.113	24.3
Meso-Co-550	6.30	31.9	0.0540	36.2
Commercial Co_3O_4	8.20	22.0	0.0560	57.6

[a] Crystallite sizes calculated from p-XRD using the Scherer equation.

mesoporous structure (Fig. 1c). These materials also have fairly high surface areas and large pore volumes, even though the surface area is greatly compromised with an increase in the final heat treatment. A similar decrease in surface area for mesoporous cobalt oxides synthesized using the same method was observed by Song et al. [7] and by Poyraz et al. [21].

Thus, one low angle diffraction line and a Type IV adsorption isotherm suggests a regular mesoporous structure with a mono-modal pore size distribution. During heat treatment, unit cell expansion and pore size enlargement was observed from TEM images (Fig. 2) and pore size distribution graphs (Fig. 1d). As summarized in Table 1, the pore size increased from 16.3 to 31.9 nm and the crystallite size also increased from 14.9 nm to 57.6 nm with increasing thermal treatment temperature.

The catalytic activity of a catalyst towards redox reactions depends on its reducibility [37]. We, therefore, performed temperature programmed reduction using hydrogen (H_2-TPR) to investigate the difference in redox properties of the mesoporous cobalt oxide catalysts. H_2-TPR profiles (Fig. 3) show that the reduction of Co_3O_4 with small particles (*meso*-Co-150 and *meso*-Co-250) occurs stepwise from Co_3O_4 to CoO and finally to Co^0 as reported in literature [38–41]. For the large sized *meso*-Co-350, *meso*-Co-450 and *meso*-Co-550 the reduction occurs via a single step to metallic cobalt, an observation previously reported by Luo et al. [42] and Spadaro et al. [43]. The first peak appearing around 246 °C corresponds to the reduction from Co^{3+} to Co^{2+} and the broader peak in the range 300–400 °C can be ascribed to the reduction of CoO to metallic cobalt.

From the H_2-TPR profiles in Fig. 3 the reduction peaks shift to a lower temperature from *meso*-Co-150 to *meso*-Co-250, indicating that the latter catalyst is easily reducible when compared to the former. Increasing the final heat temperature to 350 °C (*meso*-Co-350) leads to decreased reducibility as seen by the shift to a higher temperature for the reduction peak of *meso*-Co-350 in Fig. 3. The decreased reducibility can be attributed to the increase in particle size and decrease in surface area with an increase in final heat treatment as observed from TEM and p-XRD analyses reported in the literature [7].

3.2. Catalytic activity of catalysts and kinetic analysis of data

The catalytic reduction of 4-nitrophenol (4NP) in the presence of excess $NaBH_4$ was chosen as a model reaction. This reaction can easily be monitored by UV–vis spectrophotometry. Typical UV–vis spectra showing a decrease in absorption at wavelength of maximum absorption for 4NP at λ_{max} = 400 nm with time for a catalyzed reaction are shown in Fig. 4(a). The decrease at λ_{max} = 400 nm occurs with a simultaneously increase in absorption at λ_{max} = 300 nm corresponding to the formation of the product, 4-aminophenol. The presence of an isosbestic point in Fig. 4(a) shows that a single product is formed and therefore makes a kinetic analysis in terms of initial rates applicable.

Preliminary tests on the catalytic activity of our prepared catalysts as well as the commercial Co_3O_4 showed that *meso*-Co-550 and the commercial sample were only slightly active with a very slow reduction of 4NP, so kinetic runs were only performed for *meso*-Co-150, *meso*-Co-250, *meso*-Co-350 and *meso*-Co-450 catalysts. Kinetic traces of the reduction of 4NP over the four different mesoporous Co_3O_4 catalysts as monitored by the decrease in absorbance at λ_{max} = 400 nm are shown in Fig. 4(b). The uncatalyzed reaction shows an insignificant decrease in the amount of 4NP, while in the presence of catalyst there is a rapid decrease in the order *meso*-Co-150 > meso-Co-250 > *meso*-Co-350 > *meso*-Co-450. A plot of the experimental data according to Eq. (3) for the different catalysts gave a linear relationship (Fig. 4c), showing that the reaction follows first-order kinetics with respect to 4NP. In Eq. (1), C_0 and C_t denote the concentrations of 4NP at initial time and at time t, respectively, C_∞ is the final concentration of 4NP, while k_{app} represents the apparent (or observed) rate constant.

$$ln\left(\frac{C_t - C_\infty}{C_0 - C_\infty}\right) = k_{app} \times t \quad (1)$$

The apparent rate constant k_{app} of the reaction was determined from the temporal decay of the strong absorption of 4-nitrophenol at λ 400 nm and can be expressed through the Langmuir-Hinshelwood (L-H) Eq. (2).

$$k_{app} = \frac{k \times S \times K_{4NP}^{n}[4NP]^{n-1}(K_{BH_4^-}\left[BH_4^-\right])^{m}}{\{1 + (K_{4NP}\,[4NP])^{n} + (K_{BH_4^-}(BH_4^-)^{m}\}^{2}} \quad (2)$$

Here k is the surface rate constant, S is the total catalyst surface area, K_{4NP} and $K_{BH_4^-}$ are the adsorption constants of 4NP and borohydride respectively, n and m are the Freundlich exponents which describe the heterogeneity of the catalyst surface. The Langmuir-Hinshelwood model assumes that reaction takes place on the surface of the mesoporous cobalt oxide where both species – nitrophenol and a hydrogen species generated by borohydride – react. The interaction of borohydride with the catalyst surface is complex, with boron species formed and also adsorbed onto the surface. To simplify this complex adsorption of borohydride it is assumed that the adsorbed boron species quickly desorb irreversibly and therefore do not take part in the rate equation [44–46] and that the rate-determining step is the reaction of the surface bound species while the adsorption/desorption equilibrium is assumed to be fast [29]. The derivation of Eq. (2) is given in the Supplementary Information (Section S1).

From the Langmuir-Hinshelwood Eq. (2), the experimentally determined rate constants,k_{app}, can be used to determine the surface rate constant, k, as well as the adsorption constants for both 4NP and borohydride, if the actual surface area of the catalyst is known. We, therefore, used non-linear curve fitting with our BET surface areas (Table 1) as constants and the experimentally obtained k_{app} values when [4NP] was kept constant and when [$NaBH_4$] was kept constant to determine the parameters k, K_{4NP} and $K_{BH_4^-}$. The plots of the k_{app} values versus [4NP] and [$NaBH_4$] for the four catalysts studied are shown in Fig. 5(a) and (b) respectively. The solid lines in the two figures show the non-linear fitting curves obtained using Eq. (2). The parameters obtained from the fittings

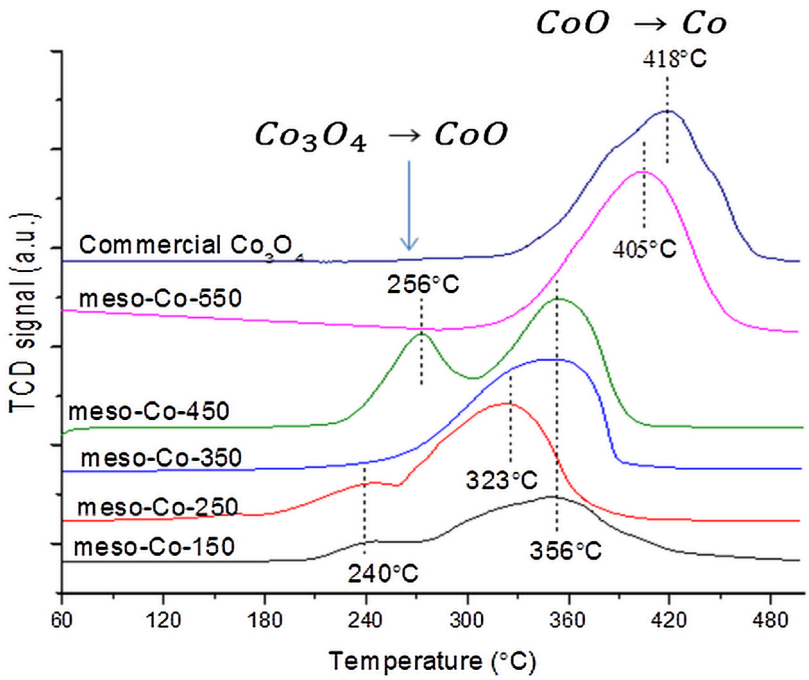

Fig. 3. H_2-TPR profiles of mesoporous cobalt oxides calcined to different final temperatures (*meso*-Co-X, X = 150, 250, 350, 450 and 550) and commercial Co_3O_4. Measurement conditions: Temperature from 30 °C to 500 °C at a rate of 10 °C/min using a stream of 10% H_2/Ar balance with a flow rate of 50.11 cm^3 STP/min.

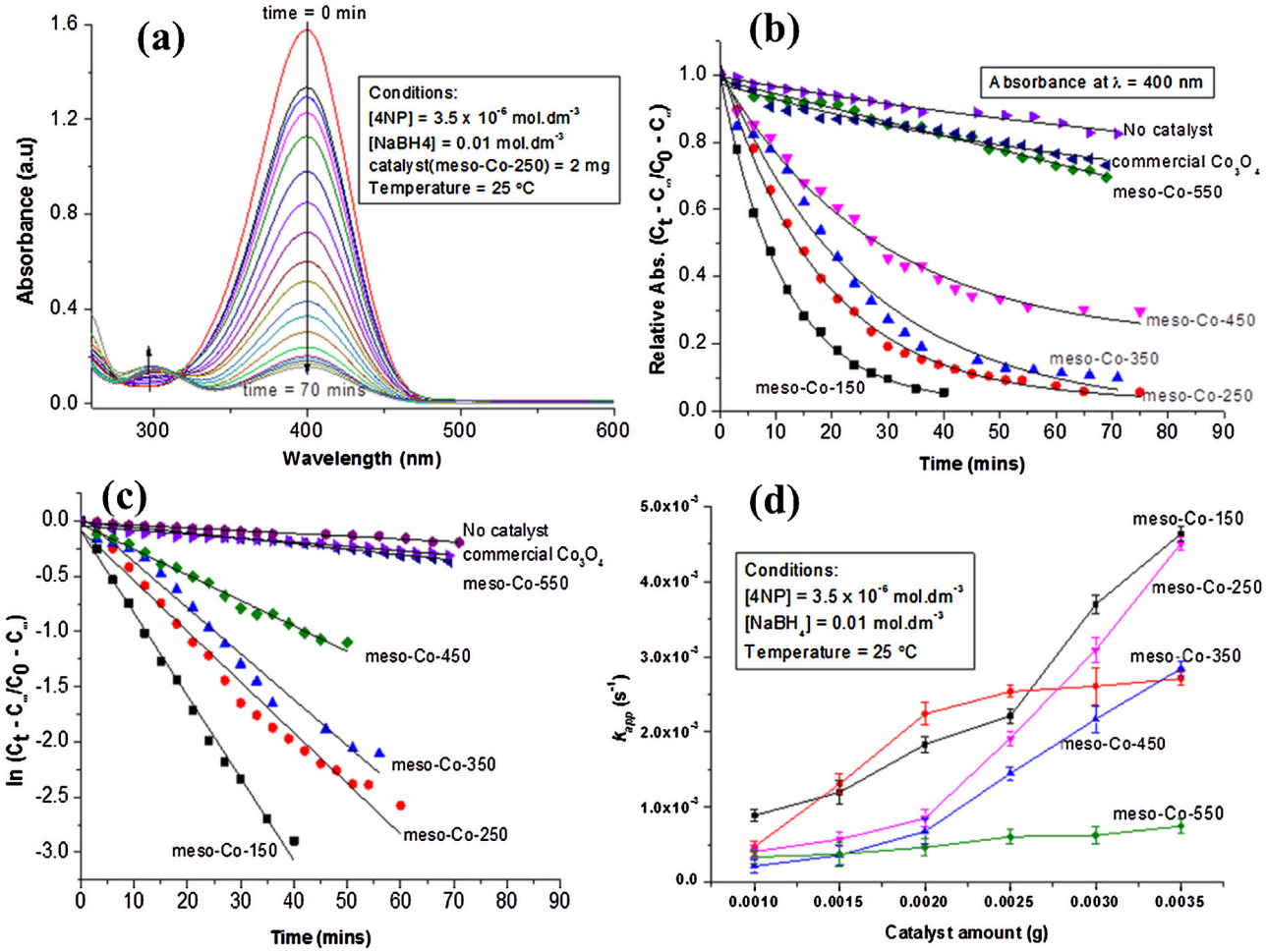

Fig. 4. (a) Typical time-resolved UV–vis spectrum of the catalyzed reduction of 4-NP over mesoporous Co_3O_4 catalysts. (b) Kinetic traces (at λ 400 nm) of the reduction of 4NP over the different mesoporous Co_3O_4 catalysts (c) Linear fits of the data in Fig. 3(b) showing *pseudo*-first order kinetics. Conditions – catalyst amount = 0.0020 g; [4NP] = 35 μM; [$NaBH_4$] = 0.01 M; Temperature = 25 °C. (d) Effect of varying the amount of catalyst on the observed rate constant.

Table 2
Parameters obtained from the fitting of the kinetic data to the L-H equation as well as values from other heterogeneous catalyzed reduction of 4NP.

Catalyst	k (mol m^{-2} s^{-1})	K_{4NP} (L mol^{-1})	$K_{BH_4^-}$ (L mol^{-1})	n	m	Reference
Meso-Co-150	5.33×10^{-6}	922 ± 40	22 ± 4	0.78 ± 0.2	1	This work
Meso-Co-250	3.55×10^{-6}	568 ± 52	15 ± 5	0.69 ± 0.1	1	
Meso-Co-350	1.02×10^{-6}	268 ± 70	14 ± 5	0.75 ± 0.1	1	
Meso-Co-450	7.80×10^{-7}	183 ± 90	8 ± 2	0.80 ± 0.3	1	
SPB-Pt	$(4.6 \pm 0.6) \times 10^{-4}$	2300 ± 500	89 ± 5	0.6 ± 0.1	1.0 ± 0.1	Wunder et al. [29]
SPB-Au	$(1.6 \pm 0.6) \times 10^{-4}$	5500 ± 1000	59 ± 5	0.6 ± 0.1	1.0 ± 0.1	
SPB-Au	$(1.89 \pm 0.28) \times 10^{-4}$	5900 ± 900	76 ± 11	0.6 ± 0.1	1.0 ± 0.1	Wunder et al. [30]
SPB-Pd	$(5.5 \pm 0.5) \times 10^{-4}$	2300 ± 400	48 ± 5	0.6 ± 0.1	1.0 ± 0.1	Kaiser et al. [31]

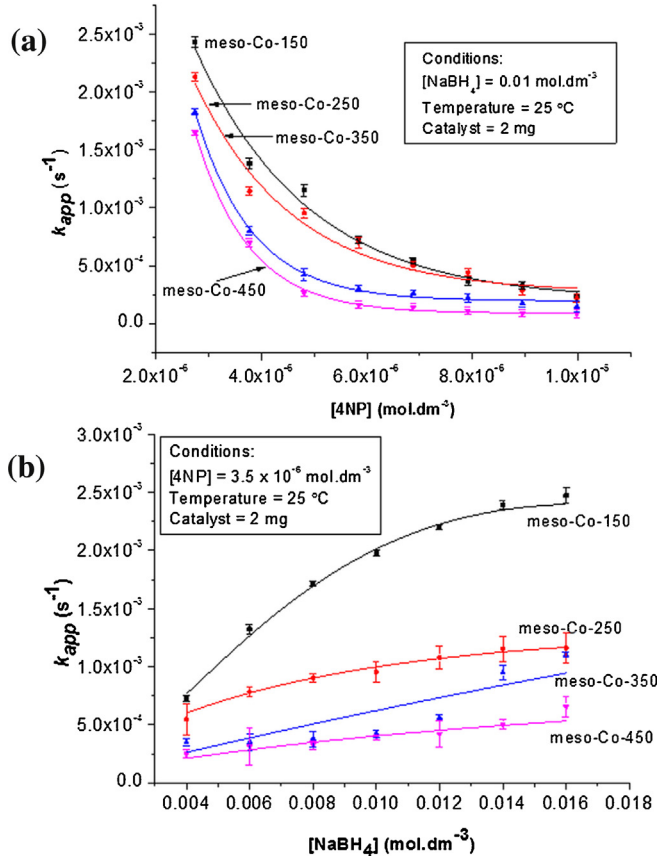

Fig. 5. Apparent rate constants as a function of (a) the concentration of 4-NP ([$NaBH_4$] = 0.01 M) and (b) the concentration of $NaBH_4$ ([4NP] = 35 μM). Catalyst amount (2 mg) and temperature (25 °C) were kept constant in both variations. Data points show the experimental k_{app} values while solid lines are the L-H fitting curves.

are summarized in Table 2 along with literature values obtained for heterogeneous catalyzed reductions of 4NP.

From Fig. 5(a), increasing the concentration of 4NP with a constant catalyst and borohydride concentration resulted in a decrease in the apparent rate constants. In contrast, an increase in the concentration of borohydride while keeping [4NP] constant resulted in an initial increase in the apparent rate constants with a subsequent leveling off indicating that there is competition between 4NP and $NaBH_4$ for the adsorption onto the catalyst surface as postulated by the Langmuir-Hinshelwood mechanism. This can be explained from the adsorption constants (K_{4NP} and $K_{BH_4^-}$) shown in Table 2, where adsorption of 4NP is significantly larger than that of borohydride, with the consequence that at high [4NP] most of the catalyst surface is occupied by 4NP leaving less surface accessible to the borohydride and, therefore, the observed decrease in the apparent rate constants. On the other hand keeping [4NP] constant while increasing borohydride concentration means initially the borohydride has more sites to adsorb onto and react with 4NP but as the concentration increases these sites get saturated and any further increase in borohydride concentration results in a leveling off as seen in Fig. 5(b).

The surface normalized rate constant denoted k in Eq. (2), which can be directly related to the rate-determining step of the reaction, was seen to increase in the order *meso*-Co-150 > *meso*-Co-250 > *meso*-Co-350 > *meso*-Co-450 (Table 2). This correlated well with the experimentally determined apparent rates, which in turn follow the trend of increasing surface areas as well as the increasing crystallite size of the catalysts. The effect of crystallite size on the catalytic activity of our mesoporous cobalt oxides is illustrated graphically in Fig. 6(a) and (b). Fig. 6(a) shows a decrease in the surface normalized rate constant with an increase in crystallite size from *meso*-Co-150 to *meso*-Co-450 and complementary increase in activation energy is shown in Fig. 6(b). The enhanced catalytic activity of *meso*-Co-150 can be explained by better dispersion of the Co_3O_4 crystallites of the smallest size, a similar observation made for Co_3O_4/CeO_2 composites by Liotta et al. [40] While there was a significant increase in the pore sizes of the catalysts from *meso*-Co-150 to *meso*-Co-450 which could result in increased diffusion of reactants, the large surface area and small crystallite size had an overall significance on the observed apparent rates. This, therefore, gives a significant insight into what final calcination temperature to use in order to obtain the optimum surface area and crystallite size of mesoporous cobalt oxides for efficient catalytic reduction of nitro-phenols.

The quality of the data obtained from L-H fitting can be assessed by plotting k_{app}[4NP] versus $\theta_{4NP}\theta_{BH_4^-}$.This relationship was derived from the rearrangement of the L-H Eq. (2) with the substitution of the surface coverage of 4NP (θ_{4NP}) and borohydride ($\theta_{BH_4^-}$).The plots are shown in the Supplementary information (Fig. S3) and show a linear relationship with the slope being the product of surface rate constant, k and the surface area, S of the mesoporous cobalt oxide catalysts. The values obtained are in agreement with the values calculated from k (from L-H fitting) and surface area S, which means that the L-H mechanism sufficiently models the reduction of 4NP with borohydride over mesoporous cobalt oxide catalysts. Other mechanisms proposed to model the catalytic activation on solid catalysts include the Eley-Rideal (E-R) [47,48] and Mars–Van Krevelen (M-vK) [49,50] mechanisms. While the M-vK mechanism mainly focuses on adsorbed oxides, hydrides also can follow a similar mechanism [49]. We therefore fitted our experimentally obtained kinetic data (k_{app}) to the E-R and M-vK mechanisms (See Supporting information, Sections S2 and S3) in order to evaluate the reliability of our proposed L-H mechanism. Our kinetic data fitted much better to the L-H mechanism ($R^2 = 0.99794$) when compared to both E-R ($R^2 = 0.75195$) and MvK ($R^2 = 0.74331$) mechanisms, with the quoted R^2 values being for *meso*-Co-150 catalyzed reactions. The results suggest that the kinetics follows the L-H mechanism rather than the other two mechanisms.

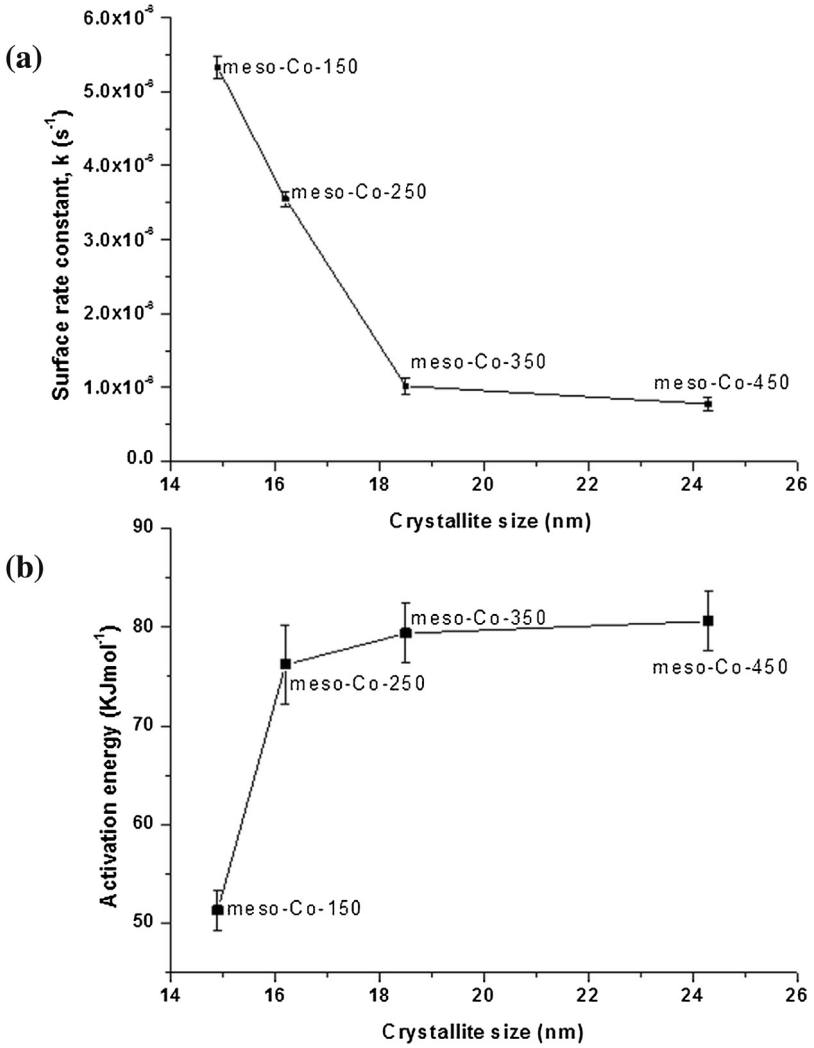

Fig. 6. The relationship between the crystallite size of each catalyst to (a) surface rate constants, k determined from L-H fitting and (b) energy of activation, E_A for the reduction of 4NP over *meso*-Co-X (X = 150, 250, 350 and 450) catalysts.

3.3. Determination of thermodynamic parameters

Thermodynamic parameters for the heterogeneous catalytic reduction of 4-nitrophenol (NP) in the presence of the different synthesized mesoporous cobalt oxides were determined by carrying out the reaction at four different temperatures (20–35 °C) and obtaining the apparent rate constants at each temperature. From the obtained apparent rate constants, we then calculated the activation energy (E_A) using the Arrhenius Eq. (3).

$$\ln\left(k_{app}\right) = \ln A - \frac{E_A}{RT} \tag{3}$$

The activation parameters, activation enthalpy ($\Delta H^{\#}$) and activation entropy ($\Delta S^{\#}$) were calculated using the Eyring Eq. (4).

$$ln\left(\frac{k_{app}}{T}\right) = -\frac{\Delta H^{\#}}{RT} + ln\left(\frac{k_B}{h}\right) + \frac{\Delta S^{\#}}{R} \tag{4}$$

From the values obtained for $\Delta H^{\#}$ and $\Delta S^{\#}$ we then calculated the Gibbs free-energy of activation $\Delta G^{\#}$. The Arrhenius and Eyring plots used to determine values for $\Delta H^{\#}$ and $\Delta S^{\#}$ are shown in the Supplementary information (Figs. S7 and S8) and all the activation parameters are summarized in Table 3.

The activation energy for *meso*-Co-150 was the lowest of all the catalysts corresponding well to the highest catalytic activity observed experimentally. The activation energies increased with final calcination temperature, with the least active *meso*-Co-550 having the highest. On comparison with the activation energies of colloidal metallic nanoparticles, which would be expected to have significantly lower E_A values and higher activities, our catalysts compared fairly well, with the *meso*-Co-150 (E_A = 51.3 kJ mol^{-1}) having an E_A value only slightly higher than Pd supported on alumina (E_A = 43.0 kJ mol^{-1}) [51] and Pd supported on spherical polyelectrolyte brushes (SPB) (E_A = 44.0 kJ mol^{-1}) [52] (Table 3). For all the catalysts, the activation enthalpy values were all positive and most of the activation entropies were negative, indicating that the reaction is endothermic and therefore energetically not favoured. The calculated $\Delta G^{\#}_{298}$ values were however, all positive for all the catalysts showing that the reaction is feasible in the presence of our catalysts as observed experimentally.

3.4. Reusability of the catalysts

To investigate the reusability of the mesoporous cobalt oxide catalyst, we repeated the reduction of 4NP with *meso*-Co-150 catalyst in four cycles and calculated the apparent rate constants for each cycle. The rate constants remained relatively unchanged even after the fourth cycle as shown in Fig. 7(a). The mesoporous nanostructure of the catalyst remained unaltered as seen in the TEM

Table 3
Activation parameters for the reduction of 4NP over *meso*-Co-X catalysts.

Catalyst	E_A (kJmol^{-1})	$\Delta H^{\#}$ (kJ mol^{-1})	$\Delta S^{\#}$ (J mol^{-1} K^{-1})	$\Delta G^{\#}_{298}$ (kJ mol^{-1})	Reference
Meso-Co-150	51.3	97.38	63.10	78.58	This work
Meso-Co-250	76.2	73.74	−20.31	79.80	
Meso-Co-350	79.4	48.40	−106.80	80.23	
Meso-Co-450	80.6	42.43	−127.47	80.42	
Pd/Al_2O_3	43.0	–	–	–	Arora et.al. [51]
[a]SPB-Pd	44.0	–	–	–	Mei et.al.[52]

[a] SPB—spherical polyelectrolyte brushes.

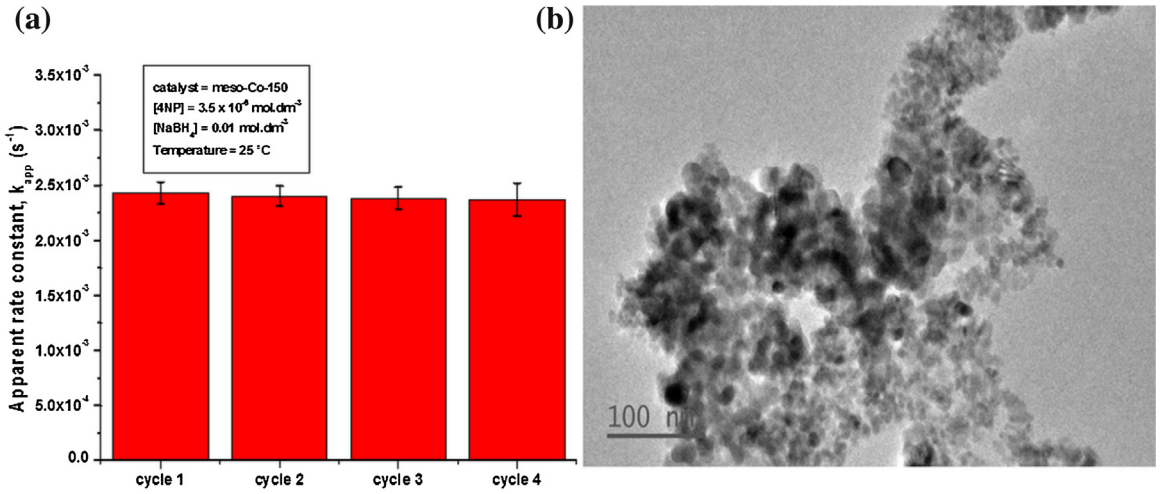

Fig. 7. (a) Graph showing the relatively unchanged k_{app} values for four cycles using *meso*-Co-150 catalyst and (b) TEM image of *meso*-Co-150 after the fourth cycle showing no significant change in the mesoporous structure and crystallite size of the catalyst.

image (Fig. 7b) showing the stability of the catalyst. Furthermore, ICP measurements showed no significant amount of cobalt in the supernatant after each run, indicating that no leaching of the catalyst into the aqueous media occurs. These results showed that the mesoporous cobalt oxide catalysts prepared are stable and can be recycled and reused in the catalytic reduction of 4NP.

4. Conclusions

Our results have shown that mesoporous cobalt oxide can be a cost effective catalyst for the reduction of 4-nitrophenol and indeed other related environmentally hazardous phenolic organic compounds. The investigation has shown that the synthesis of the catalysts is important, particularly that the final thermal treatment in the synthesis affects the surface area and pore size of the final material, both of which have direct implications on the catalytic activity of the catalyst. We have shown that calcination to high temperatures (550 °C) results in a significant decrease in the surface area of mesoporous cobalt oxide catalysts from 32.9 m^2/g for *meso*-Co-150 to 6.30 m^2/g for *meso*-Co-550 resulting in the loss of catalytic activity towards the reduction of 4-nitrophenol as seen by the decrease in the surface rate constant from 5.33×10^{-6} mol m^{-2} s^{-1} for *meso*-Co-150 to 7.80×10^{-7} mol m^{-2} s^{-1} for *meso*-Co-450. The decrease in catalytic activity corresponded to an increase in crystallite size of the catalysts from 14.9 nm for *meso*-Co-150 to 24.6 nm for *meso*-Co-450 showing a dependence of the activity to the morphology of the catalyst. It is important to understand the mechanism of the degradation of pollutants and so we have demonstrated here that using mesoporous cobalt oxide catalyst the mechanism can be explained and modelled according to the Langmuir-Hinshelwood mechanism as has been previously used for colloidal supported metal nanoparticles. The surface rate constant of 5.33×10^{-6} mol m^{-2} s^{-1} obtained from the Langmuir-Hinshelwood fitting was comparable to that obtained for palladium supported on spherical polyelectrolyte brushes of 5.5×10^{-4} mol m^{-2} s^{-1} In addition an activation energy of 51,3 kJ mol^{-1} obtained for *meso*-Co-150 was comparable to that obtained for palladium supported on spherical polyelectrolyte brushes (44.0 kJ mol^{-1}) In this respect the replacement of precious metals such as palladium, gold and platinum for the remediation of polluted water with the non-precious metals such as cobalt is of significant economic importance as it can lead to less expensive and green methods of removing organic pollutants from contaminated sources.

Conflict of interest

The authors declare no competing financial interest.

Acknowledgements

We sincerely thank the National Research Foundation (NRF, South Africa) for funding through the research grant number 85386. We also thank the University of Johannesburg as well as Shimadzu (South Africa) for the instrumentation used.

Appendix A. Supplementary data

Supplementary data associated with this article can be found, in the online version, at http://dx.doi.org/10.1016/j.apcatb.2016.05.051.

References

[1] C.T. Kresge, M.E. Leonowicz, W.J. Roth, J.C. Vartuli, J.S. Beck, Nature 359 (1992) 710–712.

[2] P. Yang, D. Zhao, D.I. Margolese, B.F. Chmelka, G.D. Stucky, Nature 396 (1998) 152–155.
[3] D. Zhao, J. Feng, Q. Huo, N. Melosh, G.H. Fredrickson, B.F. Chmelka, G.D. Stucky, Science 279 (1998) 548–552.
[4] D.E. De Vos, M. Dams, B.F. Sels, P.A. Jacobs, Chem. Rev. 102 (2002) 3615–3640.
[5] T.R. Mandlimath, B. Gopal, J. Mol. Catal. A 350 (2011) 9–15.
[6] A.S. Poyraz, S. Biswas, H.C. Genuino, S. Dharmarathna, C.-H. Kuo, S.L. Suib, Chem. Catal. Chem. 5 (2013) 920–930.
[7] W. Song, A.S. Poyraz, Y. Meng, Z. Ren, S.-Y. Chen, S.L. Suib, Chem. Mater. 26 (2014) 4629–4639.
[8] J. Rouquerol, K.S.W. Sing, P. Llewellyn, Adsorption by metal oxides, in: F. Rouquerol, J. Rouquerol, K.S.W. Sing, P. Llewellyn, G. Maurin (Eds.), Adsorption by Powders and Porous Solids, second edition, Academic Press, Oxford, 2014, pp. 393–465.
[9] Z. Wu, D. Zhao, Chem. Commun. 47 (2011) 3332–3338.
[10] P. Kumar, V.V. Guliants, Microporous Mesoporous Mater. 132 (2010) 1–14.
[11] J. Fan, C. Yu, F. Gao, J. Lei, B. Tian, L. Wang, Q. Luo, B. Tu, W. Zhou, D. Zhao, Angew. Chem. 115 (2003) 3254–3258.
[12] B. Melde, B. Johnson, Anal. Bioanal. Chem. 398 (2010) 1565–1573.
[13] T. Wagner, S. Haffer, C. Weinberger, D. Klaus, M. Tiemann, Chem. Soc. Rev. 42 (2013) 4036–4053.
[14] E. Rossinyol, J. Arbiol, F. Peiró, A. Cornet, J.R. Morante, B. Tian, T. Bo, D. Zhao, Sens. Actuators B 109 (2005) 57–63.
[15] B.J. Scott, G. Wirnsberger, G.D. Stucky, Chem. Mater. 13 (2001) 3140–3150.
[16] G. Wirnsberger, P. Yang, B.J. Scott, B.F. Chmelka, G.D. Stucky, Spectrochim. Acta A 57 (2001) 2049–2060.
[17] M.E. Davis, Nature 417 (2002) 813–821.
[18] X. Gao, S. Nie, J. Phys. Chem. B 107 (2003) 11575–11578.
[19] G.J. Soler-Illia, E.L. Crepaldi, D. Grosso, C. Sanchez, Curr. Opin. Colloid Interface Sci. 8 (2003) 109–126.
[20] Y. Wan, W.L. Zhao, Chem. Rev. 107 (2007) 2821–2860.
[21] A.S. Poyraz, C.-H. Kuo, S. Biswas, C.K. King'ondu, S.L. Suib, Nat. Commun. 4 (2013).
[22] A.S. Poyraz, W.A. Hines, C.-H. Kuo, N. Li, D.M. Perry, S.L. Suib, J. Appl. Phys. 115 (2014).
[23] A.M. Tafesh, J. Weiguny, Chem. Rev. 96 (1996) 2035–2052.
[24] N. Sahiner, H. Ozay, O. Ozay, N. Aktas, Appl. Catal. B 101 (2010) 137–143.
[25] H. Li, L. Han, J. Cooper-White, I. Kim, Green Chem. 14 (2012) 586–591.
[26] S. Saha, A. Pal, S. Kundu, S. Basu, T. Pal, Langmuir 26 (2010) 2885–2893.
[27] S. Harish, J. Mathiyarasu, K.L.N. Phani, V. Yegnaraman, Catal. Lett. 128 (2008) 197–202.
[28] K. Esumi, R. Nakamura, A. Suzuki, K. Torigoe, Langmuir 16 (2000) 7842–7846.
[29] S. Wunder, F. Polzer, Y. Lu, Y. Mei, M. Ballauff, J. Phys. Chem. C 114 (2010) 8814–8820.
[30] S. Wunder, Y. Lu, M. Albrecht, M. Ballauff, ACS Catal. 1 (2011) 908–916.
[31] J. Kaiser, L. Leppert, H. Welz, F. Polzer, S. Wunder, N. Wanderka, M. Albrecht, T. Lunkenbein, J. Breu, S. Kummel, Y. Lu, M. Ballauff, Phys. Chem. Chem. Phys. 14 (2012) 6487–6495.
[32] N.C. Antonels, R. Meijboom, Langmuir 29 (2013) 13433–13442.
[33] P. Ncube, N. Bingwa, H. Baloyi, R. Meijboom, Appl. Catal. A 495 (2015) 63–71.
[34] N. Bingwa, R. Meijboom, J. Phys. Chem. C 118 (2014) 19849–19858.
[35] Kinetic Studio, TgK Scientific Limited, Bradford-on-Avon, U.K., 2010, Transient Kinetics and Spectroscopy software.
[36] OriginPro, OriginLab Corporation, Northampton, U.K., 2014, Data Analysis and Graphing software.
[37] W. Shan, W. Shen, C. Li, Chem. Mater. 15 (2003) 4761–4767.
[38] C.-B. Wang, C.-W. Tang, S.-J. Gau, S.-H. Chien, Catal. Lett. 101 (2005) 59–63.
[39] M. Kang, M.W. Song, C.H. Lee, Appl. Catal. A 251 (2003) 143–156.
[40] L.F. Liotta, G. Di Carlo, G. Pantaleo, A.M. Venezia, G. Deganello, Appl. Catal. B 66 (2006) 217–227.
[41] L. Xue, C. Zhang, H. He, Y. Teraoka, Appl. Catal. B 75 (2007) 167–174.
[42] J.-Y. Luo, M. Meng, X. Li, X.-G. Li, Y.-Q. Zha, T.-D. Hu, Y.-N. Xie, J. Zhang, J. Catal. 254 (2008) 310–324.
[43] L. Spadaro, F. Arena, M.L. Granados, M. Ojeda, J.L.G. Fierro, F. Frusteri, J. Catal. 234 (2005) 451–462.
[44] J.S. Zhang, W.N. Delgass, T.S. Fisher, J.P. Gore, J. Power Sources 164 (2007) 772–781.
[45] S. Basu, A. Brockman, P. Gagare, Y. Zheng, P.V. Ramachandran, W.N. Delgass, J.P. Gore, J. Power Sources 188 (2009) 238–243.
[46] G. Guella, B. Patton, A. Miotello, J. Phys. Chem. C 111 (2007) 18744–18750.
[47] E.R. Williams, G.C. Jones, L. Fang, R.N. Zare, B.J. Garrison, D.W. Brenner, J. Am. Chem. Soc. 114 (1992) 3207–3210.
[48] S. Carregal-Romero, J. Peírez-Juste, P. Herveís, L.M. Liz-Marzaín, P. Mulvaney, Langmuir 26 (2009) 1271–1277.
[49] C. Doornkamp, V. Ponec, J. Molec. Catal. A 162 (2000) 19–32.
[50] A.M. Ali, E.A.C. Emanuelsson, D.A. Patterson, Appl. Catal. B 97 (2010) 168–181.
[51] S. Arora, P. Kapoor, M.L. Singla, React. Kinet. Mech. Catal. 99 (2010) 157–165.
[52] Y. Mei, Y. Lu, F. Polzer, M. Ballauff, M. Drechsler, Chem. Mater. 19 (2007) 1062–1069.